Journal of Colloid and Interface Science 534 (2019) 31–36

Contents lists available at ScienceDirect

Journal of Colloid and Interface Science

journal homepage: www.elsevier.com/locate/jcis

Regular Article

Stability of near-surface ordering of bicontinuous microemulsions in external shear-fields

Frederik Lipfert [a,b], Michael Kerscher [a,c], Stefan Mattauch [a], Henrich Frielinghaus [a,*]

[a] Jülich Centre for Neutron Science at MLZ, Forschungszentrum Jülich GmbH, Lichtenbergstrasse 1, 85747 Garching, Germany
[b] Etrality GmbH, Zillenweg 9, D-83115 Neubeuren, Germany
[c] Wacker Chemie, Franz-Alexander-Strasse 7, 84489 Burghausen, Germany

GRAPHICAL ABSTRACT

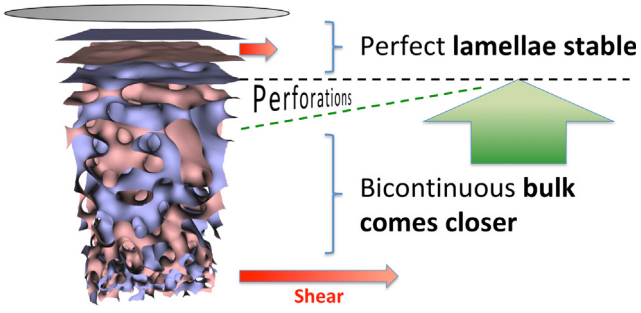

ARTICLE INFO

Article history:
Received 8 August 2018
Revised 4 September 2018
Accepted 4 September 2018
Available online 5 September 2018

Keywords:
Microemulsion
Near surface ordering
Shear field
Lubrication effect
Grazing incidence neutron scattering
Neutron reflectometry

ABSTRACT

The *lubrication* effect of bicontinuous microemulsions describes a facilitated flow along hydrophilic planar surfaces because the fluid forms lamellar domains that can slide off along each other much better than randomly ordered domains. The applicability of this effect is based on the prerequisite of the lamellar structure not being destroyed by external shear-fields. In this paper, we demonstrate that the lamellar structure is highly stable for shear rates of up to 600 s^{-1} using neutron reflectivity and grazing incidence small angle neutron scattering experiments. The transition structure that consists of perforated lamellae is attacked by the flow, and the bicontinuous microemulsion comes closer to the solid interface when shear is applied. All of this verifies the stability of the lubrication effect for technical applications.

1. Introduction

Microemulsions consist of water and oil and a surfactant that mediates between the otherwise immiscible components to form a thermodynamically stable system [1–3]. On microscopic length scales pure water and oil domains form, observable by scattering experiments [4], with the surfactant molecules as a film in between the two domains. Bicontinuous microemulsions form when nearly equal volumes of water and oil are mixed that lead to sponge-like domains hosting the other domain and vice versa.

When exposing a bicontinuous microemulsion to a planar hydrophilic surface [5], near-surface ordering happens to shape the domains lamellar next to the interface. This lamellar interphase is perfectly ordered within a depth d, and decays gradually by an increasing number of perforations to transit to the bicontinuous

* Corresponding author at: Jülich Center for Neutron Science at MLZ, Forschungszentrum Jülich GmbH, Lichtenbergstrasse 1, D-85747 Garching, Germany.
E-mail address: h.frielinghaus@fz-juelich.de (H. Frielinghaus).

https://doi.org/10.1016/j.jcis.2018.09.014
0021-9797/

bulk structure [5]. The dynamics of the lamellar surfactant membranes were about three times faster than the corresponding bulk dynamics [6] that is based on a higher number of modes being present at the interface with higher frequencies at the same time. This effect was also connected to the so-called *lubrication* effect [7] that describes a facilitated flow of lamellar domains along the solid interface. Using clay platelets as planar surfaces with limited extension, the quality of the lamellar order could be rendered [8]. Larger platelets showed faster dynamics due to more long-wavelength modes compared to the small platelets [8]. In macroscopic rheology experiments [9] the lubrication effect with varying quality of lamellar order next to clay platelets with finite dimensions could be verified. Large platelets induced much lower viscosities compared to small platelets. Using crude oils as complex fluid, the viscosity could be even decreased with respect to the bare liquid at lowered temperatures. The formation of lamellar domains adjacent to the clay particles was assumed here as well.

It remains an open question whether the lamellar interphase is stable at elevated shear rates which was inherently assumed for the lubrication effect in applications. This paper verifies the stability of the lamellar interphase as a function of shear rate using neutron reflectometry and grazing incidence small angle neutron scattering (GISANS). The observed reflectivity curves and GISANS patterns are analyzed as a function of shear rate and interpreted by a three-level structure: a perfect lamellar interphase with thickness d, a transition region with thickness ζ, and the bicontinuous bulk phase.

2. Materials and methods

2.1. Materials

N-decane was obtained from Sigma Aldrich. The non-ionic surfactant $C_{10}E_4$ was obtained from Bachem, Weil am Rhein, Germany. Heavy water was obtained from Armar chemicals, Döttingen, Switzerland. All these chemicals were used without further purification. The microemulsions consisted of 17%vol surfactant and 41.5%vol water and oil, respectively. The microemulsion was kept stable at 25 °C ± 1 K with a safe distance to the 2-phase regions of at least ±2 K. The phase diagram of the symmetric microemulsion with varying surfactant content γ is depicted in Fig. 1. Here, all materials were fully hydrogenous, and the corresponding phase diagram with heavy water needs to be shifted down by 2 K. The experimental condition is indicated by a diamond. There is the important 1-phase bicontinuous microemulsion indicated by "1" that is limited by a lamellar phase towards $\gamma \approx 19\%$. There are 2-phase coexistence regions with expelled oil or water indicated by "$\bar{2}$" and "$\underline{2}$". The 3-phase coexistence region is indicated by "3" and consists of excess oil and water with a concentrated microemulsion. Further details about phase diagrams of microemulsions with non-ionic surfactants can be found in the literature [10]. The 1-phase microemulsion forms spontaneously, and comes to quick (sub seconds) equilibrium after shaking. When the sample is kept at the equilibrium temperature, as for the neutron experiments, no phase separation occurs.

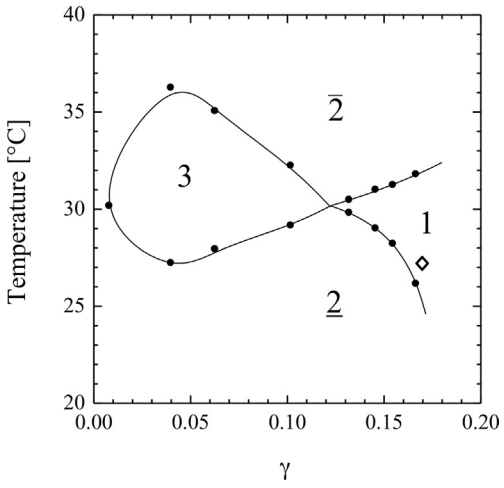

Fig. 1. Phase diagram of the symmetric microemulsion of *n*-decane, normal water and $C_{10}E_4$. The diamond indicates the experimental condition for the neutron experiments. For heavy water, the whole figure is shifted down by 2 K.

2.2. Neutron experiments

The flow cell for neutron reflectometry and grazing incidence small angle neutron scattering [5,11] hosted a polished silicon slab ($150 \times 50 \times 20$ mm^2) with a roughness better than 2 Å. It was etched before use as described in Refs. 5 and 11 to obtain hydrophilicity. The flow along the slab took place on an area of approx. 120×30 mm^2; and the gap was 0.5 mm. The cell was connected with a Luer Lock® System to a peristaltic pump. An average flow speed of up to 50 mm/s could be reached in the cell that translates to an apparent shear rate of 600 s^{-1} at the interfaces with the shear gradient in the normal direction assuming Hagen-Poiseuille flow. The cell was tempered by a water-thermostat to 25 °C, and a limited area around the pump was heated by an electric heat blower. The neutrons impinge on the silicon front face, are reflected from the solid-liquid interface, and leave through the opposite back face.

Neutron Reflectometry was conducted on the instrument MARIA at the MLZ Garching [12,13]. The neutron wavelength was 5 Å. The entrance and sample slits were 0.4×148 mm^2 and 0.4×30 mm^2 for the reflectivity data represented here. All data were normalized by a heavy water reference scan such that the total reflectivity plateau was unity. All reflectivities are given as a function of the scattering vector Q. GISANS experiments were conducted with a wavelength of 10 Å, and all slits were set to 16×2 mm^2. The scattering length density (SLD) of the overall microemulsion was 2.456×10^{-6} Å^{-2} while the SLD of silicon was 2.07×10^{-6} Å^{-2}. This resulted in a critical angle of 0.20°. The incidence angles of 0.14°, 0.16°, and 0.18° and 0.20° resulted in the scattering depths of Λ = 7632 Å, 749 Å, 1018 Å and virtually infinity (as we refer to them as nominal scattering depths). The experimental scattering depths are smeared out by resolution effects by ± 140 Å, ±270 Å, and ± 770 Å correspondingly. These problems are discussed in the literature [14,15] where even the non-linearity is taken into account for more complicated conditions. For simplicity we stay with the nominal scattering depths.

2.3. GISANS formulae

Let's assume the incoming wave is a pure evanescent wave, i.e. $\boldsymbol{k}_i = (k_{i,x}, k_{i,y}, \mathrm{i}/\Lambda)$, and the outgoing wave has negligible damping in z-direction, i.e. $\boldsymbol{k}_f = (k_{f,x}, k_{f,y}, k_{f,z})$. The scattering probability and, therefore, the scattering intensity is described by the following [16]:

$$I(\boldsymbol{k}_i, \boldsymbol{k}_f) = \left| \int d^3\boldsymbol{r}\rho(\boldsymbol{r})\exp(\mathrm{i}(\boldsymbol{k}_i - \boldsymbol{k}_f)\boldsymbol{r}) \right|^2 \quad (1)$$

in the hemisphere $z > 0$. A very basic simplification is achieved, if along the z-axis the scattering volumes are decoupled by a rather small correlation length ξ. Then, different sub-volumes of size ξ do not interfere, and the following simplification holds:

$$I(\boldsymbol{k}_i,\boldsymbol{k}_f) \approx \sum_j \exp(-2j\xi/\Lambda)\left|\int_{V^j_{\mathrm{sub}}} d^3\boldsymbol{r}\rho(\boldsymbol{r})\exp\left(\mathrm{i}(\mathrm{Re}(\boldsymbol{k}_i)-\boldsymbol{k}_f)\boldsymbol{r}\right)\right|^2 \tag{2}$$

Now we assume that two phases coexist with a probability function along the z-axis $\phi_1(z)$ for phase 1, and $\phi_2 = 1-\phi_1$. Each of them has a characteristic scattering function for the correlation volume, being $S_1(\boldsymbol{q})$ and $S_2(\boldsymbol{q})$ with $\boldsymbol{q} = \mathrm{Re}(\boldsymbol{k}_i)-\boldsymbol{k}_f$. The original sum for the compartments is replaced by an integral, and we arrive at:

$$I(\boldsymbol{q},\Lambda) \approx (S_2(\boldsymbol{q})-S_1(\boldsymbol{q}))\int_{z>0}^{\infty} dz\phi_2(z)\exp\left(-2\frac{z}{\Lambda}\right)+\frac{\Lambda}{2}S_1(\boldsymbol{q}) \tag{3}$$

So a simple Laplace transformation of the probability function $\phi_1(z)$ appears. For a profile ϕ_2 being zero between $z = 0$ and d, and an error function $\mathrm{erf}((z-d)/\zeta)$ describing a transition with a width ζ towards the bulk phase, we obtain two characteristic functions:

$$f_2(\Lambda) = \exp\left(-2\frac{d}{\Lambda}\right)\cdot\frac{\Lambda}{2}\exp\left(\frac{\zeta^2}{\Lambda^2}\right)\left(1-\mathrm{erf}\left(\frac{\zeta}{\Lambda}\right)\right) \text{ and}$$

$$f_1(\Lambda) = \frac{\Lambda}{2}-f_2(\Lambda) \tag{4}$$

The characteristic f_2 function has a linear asymptote $(\Lambda-\Lambda_0)/2$ with a virtual zero at $\Lambda_0 = 2(d+\zeta/\sqrt{\pi})$. Since the characteristic function f_2 does not reach this ideal asymptote at $\Lambda = 1000$ Å, we take the Taylor expansion at the point ($\Lambda = 1000$ Å, $d = 600$ Å, and $\zeta = 500$ Å) with the first two values being typical and the latter being in the middle of the range between 0 and 1000 Å. We arrive at the following linearization (all variables in Å):

$$\begin{aligned} f_2[\text{Å}] \approx\ & -248.6+0.5376\Lambda+0.06038\zeta+0.1066d \\ & -0.0002302\Lambda\zeta-0.0003693\Lambda d+1.530\cdot10^{-5}\zeta d \\ & +1.391\cdot10^{-7}\Lambda\zeta d \end{aligned} \tag{5}$$

From this we can obtain further simplifications for the bicontinuous intensity at $\Lambda = 1000$ Å and $d = 600$ Å:

$$f_2[\text{Å}] \approx 131.3-0.07721\zeta[\text{Å}] \tag{6}$$

This function would show a 2.4 times fold increase when ζ varies from 1000 Å to 0 Å. The corresponding function f_1 would read at the same time:

$$f_2[\text{Å}] \approx 368.7+0.07721\zeta[\text{Å}] \tag{7}$$

This corresponds to a 17% decrease of the lamellar intensity in the same range of ζ. The linearized virtual zero of the linearized equation A5 would be:

$$\Lambda_0[\text{Å}] = 584.4+0.0513\zeta[\text{Å}] \tag{8}$$

This corresponds to an 8% decrease of the lamellar depth in the same range of ζ. We know that the range of ζ might be a little shorter than assumed here, to fit the measured changes better. However, the changes give a good estimation for the theoretical description still.

3. Results and discussion

When looking at the reflectivity curves (Fig. 2) of the bicontinuous microemulsion as a function of shear, the characteristic peak at $Q = 0.028$ Å^{-1} does change neither the peak height, nor the peak width, nor the peak position dramatically [17]. A tiny change is visible for the highest shear rate of 600 s^{-1}. From the scattering geometry, we know that the Q-vector is ideally perpendicular to the solid surface and therefore represents the near-surface lamellar structure induced by the hydrophilic preparation of the silicon slab. As such, this lamellar interphase does not seem to change dramatically, when shear is applied. In model fitting, a simple Lorentzian [17] was used to describe the peak shape with the three parameters amplitude, peak width, and peak position. As one example, we displayed the correlation length in Fig. 3 that emerged from the reciprocal peak width of the fitting. Within the statistical errors, the correlation length is nearly constant. A tiny decay of a little more than 10% might be taken as a result towards highest shear rates of 600 s^{-1}.

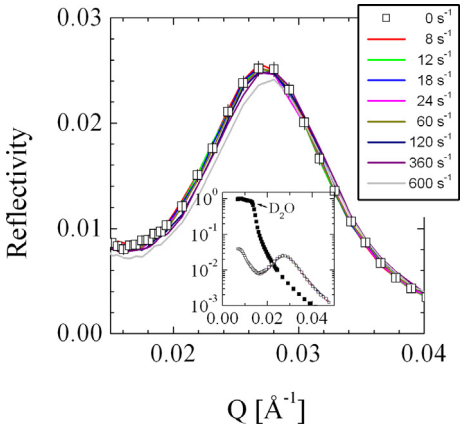

Fig. 2. (color) Neutron Reflectometry of the microemulsion at different apparent shear rates. In the inlay, the reference measurement of heavy water as calibrant is depicted. Error bars are of the symbol size. (For interpretation of the references to colour in this figure legend, the reader is referred to the web version of this article.)

The GISANS patterns were taken as a function of the scattering depth and shear rate (Fig. 4). The lamellar Bragg peak (Q_z,Q_y) ≈ (0.03 Å^{-1},0 Å^{-1}) is dominating at a scattering depth of $\Lambda = 632$ Å, although the isotropic Debye-Scherrer ring from the bicontinuous phase [18] is slightly present. The bicontinuous scattering is stronger at $\Lambda = 749$ Å, and even stronger at 1018 Å. Finally, it prevails at incidence angles larger than the critical angle of total reflection when the scattering depth is virtually infinity. This trend explains that the lamellar structure is adjacent to the solid interface and the bicontinuous phase is in the bulk volume. From the shear experiments, we can also see clearly that with stronger shear rates the bicontinuous scattering is growing. This effect is the central result that interpretation we will develop below. All GISANS patterns were analyzed [5] as a superposition of a Bragg peak and a Debye-Sherrer ring, where basically the amplitudes were the central fitting parameters after the detailed Q-dependence of the two

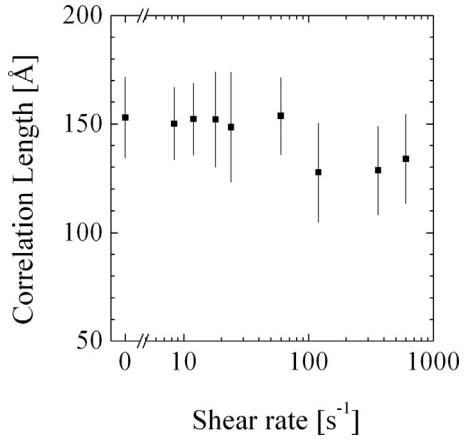

Fig. 3. The correlation length of the near-surface lamellar order as a function of the apparent shear rate.

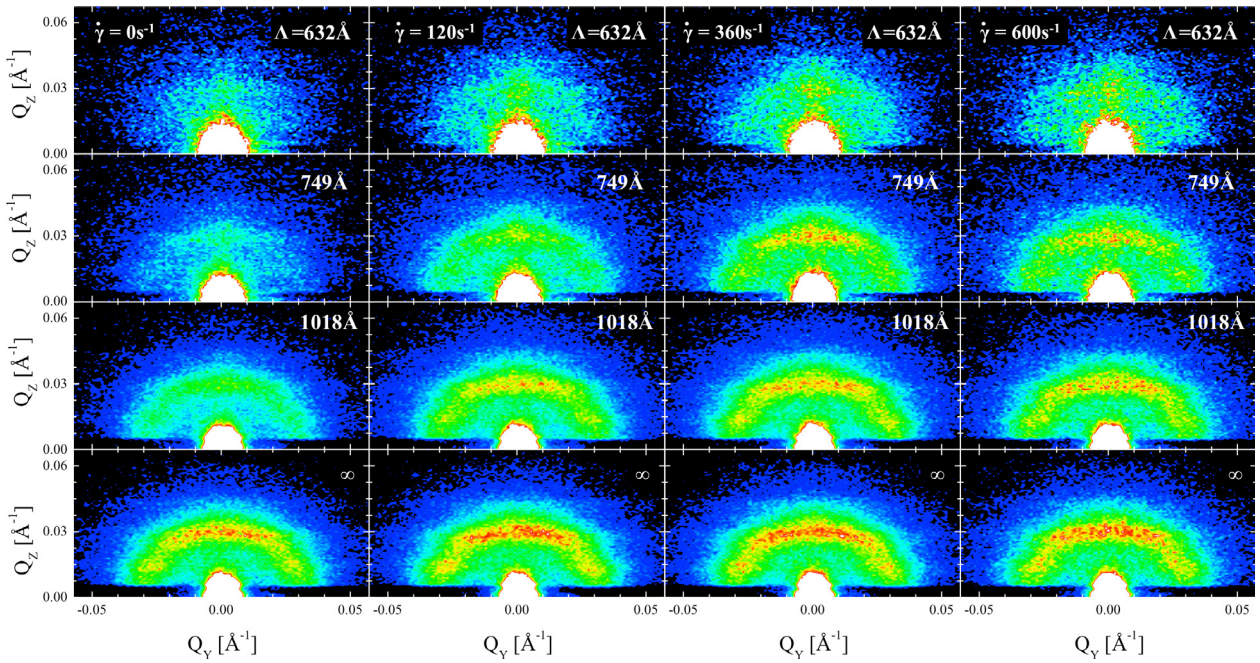

Fig. 4. (color) The grazing incidence small angle neutron scattering patterns of the microemulsion at the apparent shear rates $\dot{\gamma}$ = 0, 120, 360, and 600 s^{-1}. The patterns were described as a superposition of a Debye-Scherrer ring and a Bragg peak. (For interpretation of the references to colour in this figure legend, the reader is referred to the web version of this article.)

scattering patterns have been fixed from the dominating situations (Λ = 632 Å, no shear) and (Λ = ∞, no shear). Principal details have been given already in the literature [5]. The obtained amplitude of the Bragg peak is depicted in Fig. 5. From the two lower scattering depths Λ = 632 Å and 749 Å, we see the essential trend that the intensity grows with scattering depth, but is interpreted as nearly constant as a function of shear rate. For the highest scattering depth Λ = 1018 Å, the intensity of zero shear is nearly the same as for Λ = 749 Å. The drop with increasing shear rate at Λ = 1018 Å seems to be an effect of prevailing bicontinuous scattering. So, just statistically the Bragg peak becomes negligible here, which is the reason for the strongly decaying lamellar intensity at Λ = 1018 Å.

The corresponding intensities of the bicontinuous bulk scattering are summarized in Fig. 6. The linear dependence of this intensity with the scattering depthΛ was already used before [5]. The

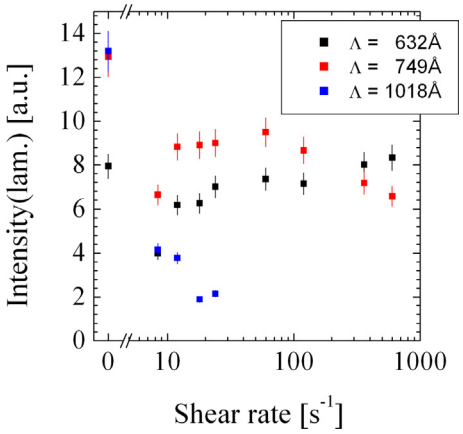

Fig. 5. (color) The intensities of the Bragg peak connected to the near-surface lamellar order for different scattering depths and apparent shear rates. (For interpretation of the references to colour in this figure legend, the reader is referred to the web version of this article.)

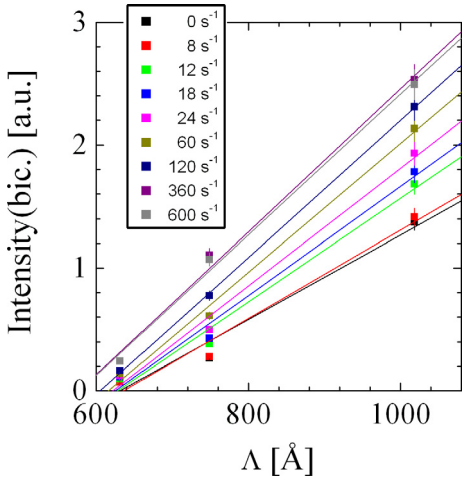

Fig. 6. (color) The intensities of the bicontinuous microemulsion as a function of the scattering depth for different apparent shear rates. (For interpretation of the references to colour in this figure legend, the reader is referred to the web version of this article.)

typical depth of the lamellar interphase obtained from the virtual zeros of Fig. 6 as a function of shear rate displays a continuous decay by approx. 7% and is statistically significant. This decay seems to agree in quantity with the correlation length (Fig. 3) of the lamellar phase. Astonishingly, the slope of Fig. 6 and simultaneously the intensity of Λ = 1018 Å grow with increasing shear rate by approx. 65%. This increase is significant and is hard to rationalize with the parameters of the lamellar structure being nearly unchanged as a function of shear rate.

4. Discussion

From previous results [5], the depth of the lamellar interphase was already established. From computer simulations, this depth

was even more precisely the depth of perfect lamellae, while the strong formation of perforations developed beyond this depth and transits into the bicontinuous structure continuously without being recognized by the GISANS experiments. The current depth of approx. 600 Å is a little larger than the previously found 400 Å, which might be connected to a better preparation of the hydrophilicty of the solid interface that would induce more order. So we have approx. 6 perfect water and oil domains (each of them 110 Å thick) at the solid interface. The short correlation length of approx. 150 Å (Fig. 3) is not much different from previous measurements [5], but now really cannot explain the overall decay of the lamellar order from the solid interface to the bulk. Also, the fitted Lorentzian corresponds more to bulk scattering that would additionally be multiplied by Q_z^2 for a pure near-surface structure (and clearly is not true for the measured data). Such simplified formalism of reflectivities of near-surface structures is connected to the classical simple Fourier transformation [19] for a reflectivity in the range of 0.01 and below, which deviates from the full theory of the Parratt formalism [16] that includes high reflectivities of nearly unity. So, the observed peak in the reflectivity does mainly result from scattering of independent lamellar sub-volumes at arbitrary depth (for us at depths of up to 600 Å). Those sub-volumes are well enough aligned to contribute to the reflectivity, but certainly do not only represent a continuous decay of structure directly at the interface with a decay length of 150 Å. As we know, the extension of the lamellar structure is approx. 600 Å.

For modeling the different intensities, the small correlation volumes of 150 Å for the lamellar and approx. 100 Å for the bicontinuous bulk phase [20] make the argumentation easier because they are much smaller than the lamellar interphase depth d of approx. 600 Å. Then, the different sub-volumes are scattering independently with the intensity mainly given by the evanescent wave as argued in more detail in the Appendix. The characteristic functions for the lamellar and the bicontinuous intensities can be linearized for typical values of (Λ = 1000 Å, d = 600 Å and ζ = 500 Å being the scattering depth, the depth of the perfect lamellar interphase and the transition range between lamellar and bicontinuous (ideally taken by perforations of a lamellar structure before the structure becomes bicontinuous) all explained in Fig. 7). From them, we obtain a linearized behavior for the lamellar and the bicontinuous intensities f_2 and f_1 as a function of ζ that match approximately the experimental findings (see Appendix). Also, the depth of the lamellar interphase d is derived in a linearized

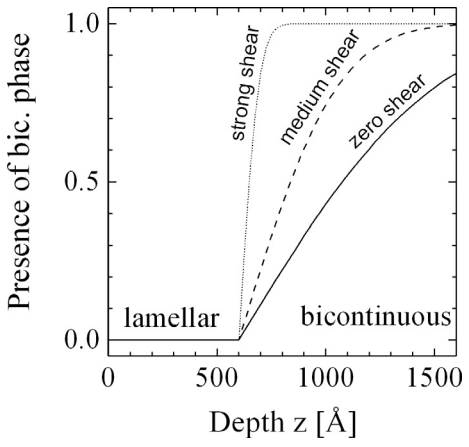

Fig. 7. Interpretation of the neutron reflectometry and grazing incidence small angle neutron scattering data for the bicontinuous microemulsion under shear. The transition between the lamellar and the bicontinuous structure is continuous with a different transition depth ζ, while the ideal lamellar interphase depth d = 600 Å is rather constant.

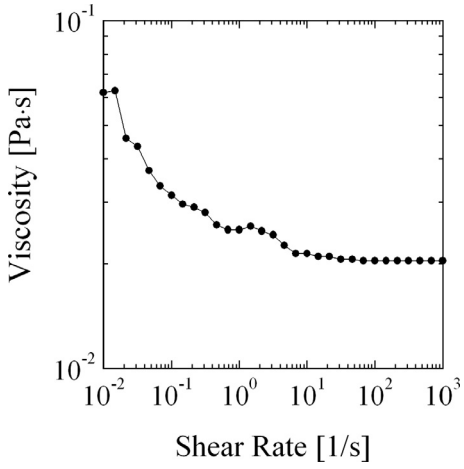

Fig. 8. The viscosity of the bicontinuous microemulsion as a function of the shear rate. At low shear rates <5 s^{-1} the Brownian motion perturbs the measurement, while at higher shear rates absolutely no indication of shear thinning is observed.

way, and the approximate behavior is confirmed. From that, we can confirm that the transition range ζ lies approximately in the range of 1000 Å for no shear to 0 Å for the maximum shear.

Following previous argumentations, the perfect lamellae stay untouched by the shear while the transition range shortens and brings the bicontinuous structure closer to the solid interface. This explains plastically the nearly constant lamellar intensity while the bicontinuous intensity increases.

The here-discussed induced lamellar order of microemulsions by planar hydrophilic surfaces (at the interface [5] and all over the volume [21]) can also be induced all over the volume by shear gradients [22]. Also then, the normal direction of the lamellae would be in the direction of the shear gradient as observed experimentally [22]. But this observation is usually coinciding with shear thinning, a considerably decreasing viscosity in the range of the applied shear rates [22]. From our system, we see that there is no shear thinning in the range of applied shear rates (Fig. 8). The decay of viscosity at really low shear rates results from the Brownian motion that is faster than the imposed shear for Deborah numbers bigger than unity [23,24]. The relaxation time of whole coherence volumes of the size $(2\xi)^3 \approx (200\ \text{Å})^3$ is in the range of seconds [25] and corresponds to our transition shear rate of approx. 5 s^{-1}. Another relaxation on the level of a single domain with the size $d/2 \approx 100$ Å is connected to stalk formation and release [25] on the order of milliseconds. At corresponding shear rates of larger than approx. 1000 s^{-1} the viscosity decreases dramatically [22,25,26,27]. In polymeric microemulsions [28] the shear-induced lamellar structure might form elongated regions of enrichments that resemble shear-banding structures [29]. The high shear state is discussed as a state under duress that is out of equilibrium in terms of surface per volume arising from the typical area per head group [20] and eventually leads to phase separation.

5. Conclusion

Apart from the mathematical modeling, the observations describe a rather persistent lamellar interphase with a rather constant depth. The shear narrows the transition zone between perfect lamellar and bicontinuous structure, which means that the bicontinuous disordered phase comes closer and appears stronger in the GISANS scattering while the lamellar structure stays unchanged as seen in the reflectometry and GISANS patterns.

For the interpretation of rheology experiments on 1%vol clay particles dispersed in bicontinuous microemulsions [9] it was

inherently assumed that a lamellar structure forms a stable structure along the clay particles independently of shear that explains a facilitated flow along the platelets, the so-called *lubrication* effect. With this manuscript, we have safely verified that shear rates of up to 600 s^{-1} do not destroy the near surface lamellar ordering of bicontinuous microemulsions.

Only on the level of perforated lamellae [5] that explicitly explains the realization of transiting order from lamellar to bicontinuous, the shear seems to attack the degree of order. This explicit destruction of the intermediate structure, the perforated lamellar structure, is considerably different from shear thinning samples that tend to form more lamellar order all over the volume [22]. We know that shear rates greater than approx. 1000–3000 s^{-1} [22,25–27] lead to dynamically stable enhanced areas per surfactant head groups [20], i.e. microemulsions with enhanced interfaces between the water and oil domains that can be called intermediates between microemulsions and emulsions [28]. So in terms of shear rates not extremely higher than 600 s^{-1} the overall stability of microemulsions is attacked on a more molecular level, while below 600 s^{-1} our bicontinuous microemulsion with the surface induced ordering but without shear thinning seems to be a rather stable arrangement. This is an important statement for the lubrication effect in terms of industrial applications, and would not change for shear thinning systems in general.

References

[1] R. Strey, Coll. Polym. Sci. 272 (1994) 1005–1019.
[2] M.S. Leaver, U. Olsson, H. Wennerström, R. Strey, U. Würz, J. Chem. Soc. Faraday Trans. 91 (1995) 4269–4274.
[3] S. Engelskirchen, N. Elsner, T. Sottmann, R. Strey, J. Coll. Interf. Sci. 312 (2007) 114–121.
[4] L. Magid, P. Butler, K. Payne, R. Strey, J. Appl. Cryst. 21 (1988) 832–834.
[5] M. Kerscher, P. Busch, S. Mattauch, H. Frielinghaus, D. Richter, M. Belushkin, G. Gompper, Phys. Rev. E 83 (2011) 030401.
[6] H. Frielinghaus, M. Kerscher, O. Holderer, M. Monkenbusch, D. Richter, Phys. Rev. E 85 (2012) 041408.
[7] N. Gov, A.G. Zilman, S. Safran, Phys. Rev. E 70 (2004) 011104.
[8] F. Lipfert, O. Holderer, H. Frielinghaus, M.-S. Appavou, C. Do, M. Ohl, D. Richter, Nanoscale 7 (2015) 2578–2586.
[9] M. Gvaramia, G. Mangiapia, V. Pipich, M.-S. Appavou, S. Jaksch, O. Holderer, M. D. Rukhadze, H. Frielinghaus, Sci. Rep. (2018) (in press).
[10] R. Strey, Ber. Bunsenges. Phys. Chem. 97 (1993) 742–746.
[11] S. Jaksch, F. Lipfert, A. Koutsioubas, S. Mattauch, O. Holderer, O. Ivanova, H. Frielinghaus, S. Hertrich, S.F. Fischer, B. Nickel, Phys. Rev. E 91 (2015) 022716.
[12] S. Mattauch, A. Koutsioubas, S. Pütter, J. large-scale res. facil., <https://doi.org/10.17815/jlsrf-1-29>
[13] S. Mattauch, A. Koutsioubas, U. Rücker, D. Korolkov, V. Fracassi, J. Daemen, R. Schmitz, K. Bussmann, F. Suxdorf, M. Wagener, P. Kämmerling, H. Kleines, L. Fleischhauer-Fuß, M. Bednareck, V. Ossoviy, A. Nebel, P. Stronciwilk, S. Staringer, M. Gödel, A. Richter, H. Kusche, T. Kohnke, A. Ioffe, E. Babcock, Z. Salhi, T. Bruckel, J. Appl. Cryst. 51 (2018) 646–654.
[14] S. Nouhi, M.S. Hellsing, V. Kapaklis, A.R. Rennie, J. Appl. Cryst. 50 (2017) 1066–1074.
[15] F.A. Adlmann, J. Herbel, A. Korolkovas, A. Bliersbach, B. Toperverg, W. van Herck, G.K. Pálsson, B. Kitchen, M. Wolff, J. Phys. Condens. Matter 30 (2018) 165901.
[16] P.S. Pershan, M.L. Schlosssman, Liquid Surfaces and Interfaces, Cambridge University Press, Cambridge, 2012.
[17] H. Frielinghaus, F. Lipfert, S. Mattauch, JPS conference proceedings (2018) (submitted for publication).
[18] M. Teubner, R. Strey, J. Chem. Phys. 87 (1987) 3195–3200.
[19] R.-J. Roe, Methods of X-ray and Neutron Scattering in Polymer Science, Oxford University Press, Oxford, 2000.
[20] T. Sottmann, R. Strey, S.-H. Chen, J. Chem. Phys. 106 (1997) 6483–6491.
[21] M. Gvaramia, G. Mangiapia, P. Falus, M. Ohl, O. Holderer, H. Frielinghaus, J. Coll. Interf. Sci. 525 (2018) 161–165.
[22] L. Porcar, W.A. Hamilton, P.D. Butler, G.G. Warr, Langmuir 19 (2003) 10779–10794.
[23] M. Reiner, Phys. Today 17 (1964). 62-62.
[24] J.W. Goodwin, R.W. Hughes, Rheology for chemists: an introduction, RSC Publishing, Cambridge, 2008.
[25] M. Kotlarchyk, E.Y. Sheu, M. Capel, Phys. Rev. A 46 (1992) 928–939.
[26] M.A. Bolzinger-Thevenin, J.L. Grossiord, M.C. Poelman, Langmuir 15 (1999) 2307–2315.
[27] Internal communication on rheology SANS experiments with steady shear in cylinder geometry on similar microemulsions as of this paper.
[28] K. Krishnan, K. Almdal, W.R. Burghardt, T.P. Lodge, F.S. Bates, Phys. Rev. Lett. 87 (2001) 098301.
[29] J.K.G. Dhont, M.P. Lettinga, Z. Dogic, T.A.J. Lenstra, H. Wang, S. Rathgeber, P. Carletto, L. Willner, H. Frielinghaus, P. Lindner, Faraday Disc. 123 (2003) 157–172.